ACES Asian Chemical Editorial Society

doi.org/10.1002/cnma.202400028

CHEMNANOMAT
Research Article

www.chemnanomat.org

Non-Covalent Functionalization of Magnetic Carbon Nanotubes with Fmoc Amino Acid-Modified Polyethylene Glycol

Fusun Sevval Murat,[a] Ö. Zeynep Güner-Yılmaz,[a] Serdar Bozoglu,[b] Saime Batirel,[c] Elif Baysak,[d] Gürkan Hizal,[d] Nilgun Karatepe,[b] and Fatma Seniha Güner*[a, e]

Once dispersion and cytotoxicity issues are resolved, it has been proven that carbon nanotubes (CNTs) have great advantages in biomedical applications due to their unique properties. In this study, the superiority of carbon nanotubes was combined with magnetic targeting strategies, and a solution to the distribution problem in the aqueous media of the resulting CNTs decorated with iron oxide (mCNTs) was sought. A non-covalent functionalization approach has been utilized to overcome this fundamental drawback of mCNTs. Conjugates of polyethylene glycol monomethyl ether and 9- fluorenyl methyl chloroformate (Fmoc) amino acids were used to coat the lateral surfaces of mCNTs, making them more water-soluble. The selected Fmoc amino acids have different numbers of aromatic rings, which is known to affect the coating efficiency in non-covalent functionalization and therefore, the dispersion behavior of the CNTs. Their coating yields, dispersion behaviors, magnetism, charge, and size properties have been determined. All coated mCNT samples displayed superparamagnetic behavior. Dispersion tests showed a promise to increase the stability of mCNTs with this approach. Moreover, we demonstrated that the functionalization of mCNTs affects cell viability in a dose-dependent manner. The main finding of this study is that mCNTs can be successfully functionalized with Fmoc amino acid-modified polyethylene glycol.

Introduction

CNTs have been revealed as excellent candidates to use in cancer diagnosis and treatment because of their exceptional properties like high aspect ratio, excellent chemical stability, excellent biological activity, and good cell membrane penetrability.[1] Owing to their hollow structure and ultrahigh surface area, CNTs provide a high amount of loading capacity for active agents such as drugs,[2–4] nanoparticles,[5–7] biological species,[5] etc. Also, the CNTs' inner cavity protects structures that can deteriorate in a biological environment. Importantly, possessing rich surface chemistry endows CNTs' multifunctionality for theragnostic applications.

The magnetization of CNTs is remarkable since it expands the usage area and adds new characteristics highlighting many good features of CNTs.[8] The use of magnetic nanoparticles for the surface functionalization of CNTs creates an opportunity to progress in many fields such as biomedical imaging[9–12] and targeted drug delivery.[13–15] Magnetic delivery, provided using an external magnetic field, has attracted a great deal of attention in biomedical applications. Guiding drug-loaded nanoparticles (NPs) through human vascular access via these magnetic fields can ensure a faster sequence to tumor cells and reduce the needed drug dosage for treatment.[16] With this objective, it can be foreseen that mCNTs have the potency to give a new point of view for drug delivery research due to their ability to target a variety of therapeutic and diagnostic agents at specified tissues.[12,17] Improving the accumulation of NPs in desired sites and thus the increase in uptake efficiency allows for reducing drug dosage and side effects.

Although mCNTs accommodate unique properties in means of drug delivery due to their structure, they have a few drawbacks that need attention. The primary issue that must be overcome is that mCNTs perform low solubility in aqueous media because of their hydrophobic nature, and therefore they tend to agglomerate in biological environments, which results

[a] F. Sevval Murat, Ö. Z. Güner-Yılmaz, Prof. Dr. F. Seniha Güner
Department of Chemical Engineering
Istanbul Technical University
Istanbul 34469 Turkey
E-mail: guners@itu.edu.tr
seniha.guner@sabanciuniv.edu

[b] S. Bozoglu, Prof. Dr. N. Karatepe
Energy Institute, Renewable Energy Division
Istanbul Technical University
Istanbul 34469 Turkey

[c] Assoc. Prof. S. Batirel
School of Medicine, Department of Medical Biochemistry
Marmara University
Istanbul 34854 Turkey

[d] E. Baysak, Prof. Dr. G. Hizal
Department of Chemistry
Istanbul Technical University
Istanbul 34469 Turkey

[e] Prof. Dr. F. Seniha Güner
Nanotechnology Research and Application Center (SUNUM)
Sabancı University
Istanbul 34956 Turkey

Supporting information for this article is available on the WWW under https://doi.org/10.1002/cnma.202400028

in them being assigned as toxic clusters by the reticuloendothelial system. Many in vitro research indicates outcomes such as oxidative stress[18,19] or apoptosis/necrosis[20] caused by the high cytotoxicity levels of pristine graphene materials. To rectify these toxic results, covalent or non-covalent functionalization of mCNTs with bioavailable and hydrophilic materials could be used, dispersing mCNTs in aqueous solutions and preventing them from forming agglomerates since the surface modification for increased solubility is a proven method for many nanoparticles.[21–23] Covalent functionalization occurs via transforming sp2 carbon atoms into sp3 carbon atoms in the lateral area of mCNTs, consequently changing the number of valence electrons on the side walls. This results in a distortion in the symmetry of the structure and a decrease in the optical, chemical, and physical advantages of mCNTs.[24] On the other hand, non-covalent functionalization is preferable since it can retain the surface properties. Non-covalent functionalization is promising to enable dispersion while lowering toxicity levels remarkably by forming π–π stackings.[25] To modify the sidewalls of CNTs, there have been numerous groups of chemicals tested, and examples of them include saccharides and polysaccharides,[26–28] proteins, nucleic acids,[29–31] and conjugated polymers.[32–34]

An approach of non-covalent functionalization with a biocompatible polymer is tried in this research to restrain the agglomeration of mCNTs and to reduce their toxicity levels. Among the appropriate polymers, poly(ethylene glycol) (PEG) is chosen as its competence is biocompatible, flexible, and hydrophilic. In our previous study, non-covalent pyrene-PEG coatings of CNTs achieved in vitro biocompatibility.[35] We show that the number of single-walled carbon nanotubes (SWCNTs) coated by pyrene-PEG was highly dependent on the length of pyrene-bearing PEG polymers. In this work, towards attaining bondage with mCNT side walls, PEG is conjugated with Fmoc amino acids. Fmoc amino acid derivatives are chosen since the fluorenyl groups and aromatic side chains in their structure are highly prone to attach to the graphitic surface of the CNTs whereas, the carboxylate fragment of them procures an overall negative charge.[36,37]

In this study, we aim to develop a new magnetic nanocarrier for biomedical applications. Unlike our previous studies, in this study, we questioned whether the walls of CNTs decorated with iron oxide could be coated with PEG conjugated with Fmoc amino acids, and even if coated, it would be efficient. According to our knowledge, a study with a similar motivation has not been published in the literature before. For this purpose, we first achieved the synthesis of mCNTs. Then, conjugation of PEG and Fmoc amino acids, cysteine (Fmoc–Cys) and tryptophan (Fmoc-Trp), is done to form functional groups. Non-covalent functionalization is applied, retaining the needed properties of the mCNT by protecting sp2 bonds on its sidewalls. Additionally, to obtain information about the effect of the chain length of the polymer on the coating yield, PEG with two different molecular weights (Mw: 5 kDa (PEG_{5000}) and 12 kDa (PEG_{12000})) is included. The coating efficacy and the solubility behavior of functionalized mCNTs are observed. Lastly, the toxicity of functionalized mCNTs on human fibroblast cells was evaluated. The overall results of this study have given important data that CNTs decorated with iron oxide may be used in therapeutic applications such as cancer research and therapy after functionalization with Fmoc amino acids.

Results and Discussion

Characterization of Synthesized mCNTs

Raman spectra of the mCNTs are presented in Figure 1. The peak at 685 cm^{-1}, also known as A_{1g} mode, belongs to the stretching vibrations of Fe^{3+} and O^{2-} in the tetrahedral site of spinel structure in magnetite (Fe_3O_4) which is compatible with the X-ray powder diffraction (XRD) pattern of iron oxide nanoparticles (IONs) (Figure S1). A group of peaks observed at approximately 213, 270, 387, 486, and 585 cm^{-1} belongs to the stretching vibrations between Fe and O in hematite (Fe_2O_3). The presence of Fe_2O_3 can be associated with the oxidation of magnetite to hematite due to a high-power laser during the measurement.[38–40] The peak at approximately 142 cm^{-1} is called RBM mode and the characteristic peak of SWCNT structure.[41,42]

The formation of SWCNT synthesis is shown with Field Emission Gun Scanning Electron Microscopy (FEG-SEM), demonstrating the exact shape of mCNTs. From the FEG-SEM images in Figure 2, it is seen that for SWCNT the formation fluidized-bed chemical vapor deposition (CVD) method was successful.

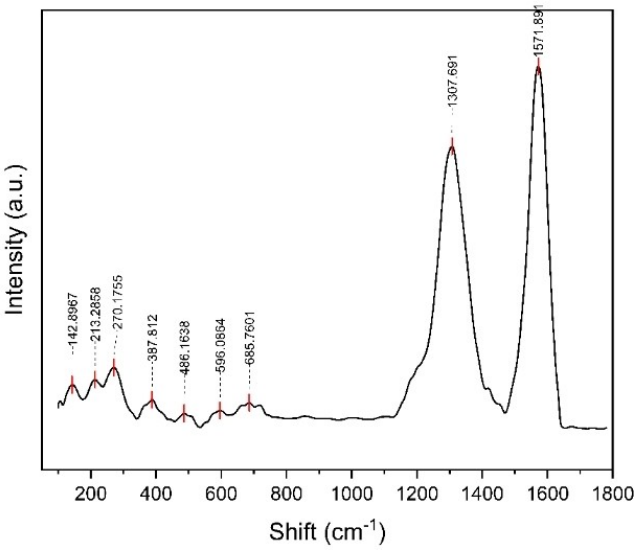

Figure 1. Raman spectra mCNTs.

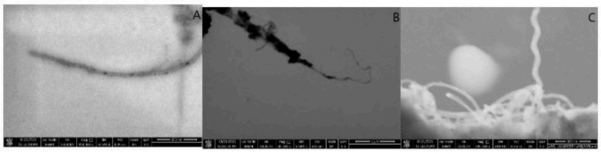

Figure 2. FEG-SEM images of mCNTs A) scale bar: 200 nm, B) scale bar: 1 μm, C) scale bar: 300 nm.

Nanotubes possess a high aspect ratio, resulting in a morphology that can be approximated as 1-D as seen in Figure 2A–B, The IONs visible in Figure 2B indicate a successful modification of the SWCNTs.

Characterization of PEG-Fmoc Amino Acids Complexes

Fourier-transform infrared (FTIR) spectroscopy and proton nuclear magnetic resonance (^{1}H NMR) analysis were applied to prove the success of direct esterification between fluorenyl groups of Fmoc amino acid and PEG. With FTIR results, we aimed to find characteristic peaks of PEG and Fmoc amino acids, proving the existence of both molecules in the complex. FTIR spectrum of Fmoc–Cys conjugated with PEG_{5000} (Cys5) is shown in Figure 3, while the other spectra for Fmoc-Trp conjugated with PEG5000 (Trp5), Fmoc-Trp conjugated with PEG12000 (Trp12), and Fmoc–Cys conjugated with PEG12000 (Cys12) are given in Supplementary Figures S2–S4. The peaks observed around 2880 cm^{-1} are caused by CH_2CH_2O- structure within the PEG molecules,[43] whereas the peaks at 1740 cm^{-1} are created by the carbonyl carbamate groups in Fmoc amino acid molecules. The peak at 1669 cm^{-1} is only seen in Fmoc amino acid samples and not in conjugates, presenting the carboxylic acid structure,[44] and proving the reduction of Fmoc amino acid complexes during esterification. Peaks formed by PEG are dense compared to those created by Fmoc amino acid molecules because of the higher molecular weight of PEG.

^{1}H NMR result of the Cys5 complex is given in Figure 4, while the other spectra are shown in Supplementary Figures S5–S7. In all spectra signals at δ 3.5–4 ppm are attributed to the repeating CH_2 units in PEG.[35,45] The multiple signals at δ 7.40–7.80 ppm are assigned to the benzene ring of Fmoc.[46] Specific cysteine and tryptophan structure peaks are marked in related spectra given in Figures 4 and S5–S7.[47] Both ^{1}H NMR and FTIR results contain characteristic markers for PEG and Fmoc amino acid structures in a briefer purview. Therefore, complex formation is successfully proven.

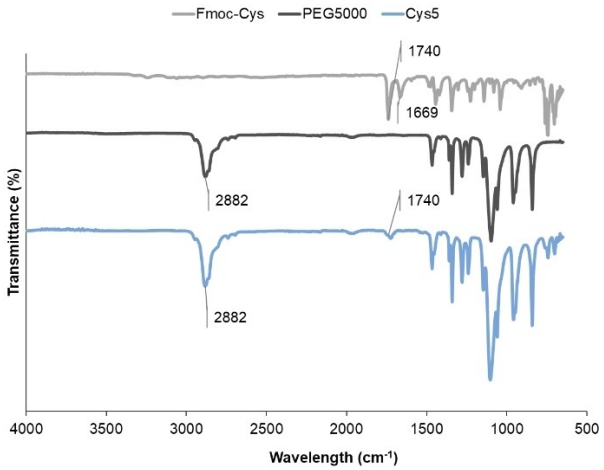

Figure 3. FTIR spectra of Fmoc–Cys, PEG_{5000}, and Cys5.

Surface Functionalization of mCNTs with PEG-Fmoc Amino Acid Complexes

As reported in the literature,[35,48,49] after π − π stacking interactions of aromatic groups on CNT sidewalls, the absorption intensity of the aromatic groups decreased drastically. Fmoc amino acid structures are natural absorbents of UV light between 250 and 330 nm due to emission from fluorenyl excimer species.[50,51] After the surface functionalization of the mCNTs, the hydrophobic ends in the aromatic groups of the Fmoc amino acid molecules interact with the surface of the mCNT. This phenomenon results in the fading of the fluorescence of the Fmoc amino acid. Therefore, comparing the amount of UV absorbance of mCNTs coated with PEG-Fmoc-amino acid and solely PEG-Fmoc-amino acid conjugates unfolds whether functionalization was achieved or not. In this work, fluorescence spectra are used to exhibit the UV absorbance quanta, and the findings for mCNTs coated with Cys5 (mCNT-Cys5) are given in Figure 5, and other samples (mCNTs coated with Trp5 (mCNT-Trp5), Trp12 (mCNT-Trp12), and Cys12 (mCNT-Cys12)) are shown in Supplementary Figures S8–S10. For all the PEG-Fmoc-*X* samples, the absorption intensity at 315–319 nm has lowered after the mCNT functionalization. Consequently, all PEG-Fmoc-*X* conjugates that we tested in this analysis were capable of coating mCNT surfaces.

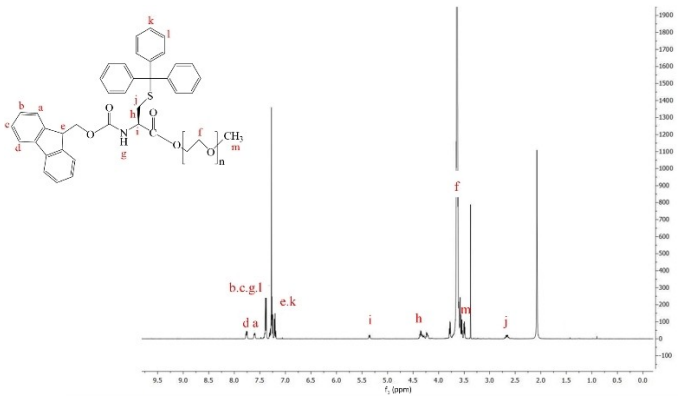

Figure 4. ^{1}H NMR characterization of Cys5.

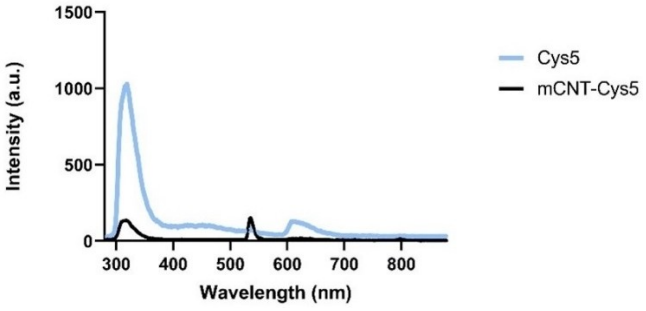

Figure 5. Fluorescence spectra of mCNT samples coated with Cys5.

Comparison of Functionalization Yields Between Functional Groups

All Fmoc-*X* kinds tend to be absorbed by graphene-like surfaces due to the aromatic fluorenyl groups within their structure. However, their level of coating capabilities differs. Therefore, several researchers are contrasting Fmoc-*X*s in terms of their success in CNT coating, and in these researches, Fmoc-Trp has been stated to be the best choice.[50] However, we hypothesized Fmoc–Cys to be a possible suitable alternative for Fmoc-Trp since the Fmoc–Cys structure has more aromatic groups within itself compared to tryptophan. These hydrophobic aromatic groups are presumed to interact with mCNTs strongly, forming π–π stackings with higher energy. To contrast the coating yields of Fmoc–Cys and Fmoc-Trp, thermogravimetric analysis (TGA) was applied with a temperature range of 30–800 °C. The purpose of choosing 800 °C as the maximum point was that mCNTs were thermally stable at that point.[52] However, PEG-Fmoc-*X* complexes degrade thermally in this temperature range. So, by applying this amount of temperature, how much functional group a sample consists of can be determined. The temperature derivative of the degradation process was observed to be variational, as given in Supplementary Figure S11. According to the former work concerning the thermal stability of Fmoc-*X*s, the slight weight losses up until 250 °C are interpreted as the degradation of Fmoc–Cys and Fmoc-Trp.[53,54] The steep curve between 250–450 °C was arrogated as the degradation of the PEG structure which conforms to previous literature.[55–57] Thermal degradation of PEG chains produced striking curves compared to Fmoc-*X* molecules due to their higher molecular mass. SWCNT was also used as a comparison sample to determine the effect of iron oxide decoration on CNT walls on thermal behavior. Every sample has been subjected to TGA 3 times. The mean values of thermal degradation percentages are given in Figure 6, with standard deviations presented. As one sees in Figure 6, the weight loss for SWCNT is negligible, with a value of only 2.7 %. Nevertheless, the weight loss for mCNTs has a percentage of 8.6 %. The increase in weight loss of mCNT can be explained firstly by the removal of tightly bound physiosorbed water.[58] Moreover, a phase transition occurs from Fe_3O_4 to hematite (FeO) between 570–700 °C, which may be associated with the additional weight loss in mCNT.[59] Hence, the thermal degradation values for samples consisting of coated mCNTs are calculated by subtracting the amount of weight loss caused by mCNT degradation. For conjugates containing both PEG_{5000} and PEG_{12000}, Fmoc–Cys have shown similar weight losses with the samples containing Fmoc-Trp. The thermal degradation percentages for Cys5 and Trp5 were 17.6 % and 13.8 %, respectively. As for PEG_{12000}-Fmoc-*X* conjugates, 56.8 % of samples consisting of Fmoc–Cys and 58.7 % of Fmoc-Trp degraded thermally. Even though the additional tertiary aromatic rings of Fmoc–Cys had promised a better behavior, it performed a similar coating performance with Fmoc-Trp. This phenomenon is assumed to result from the bulky aromatic ring structure of Fmoc–Cys having a relatively high diameter compared to the aromatic rings in the Fmoc-Trp form. This higher diameter is hypothesized to consume more volume, covering neighbor C atoms in the mCNT surface, and preventing attachment of extra functional groups. Another possible reason for Fmoc–Cys to bond less efficiently to mCNTs is that, according to our previously published simulation data,[37] Fmoc–Cys molecules tend to agglomerate within themselves in aqueous media. Since tetrahydrofuran (THF) is also a polar solvent similar to water, Fmoc–Cys molecules might have formed agglomerates during the coating process. The leading cause for this aggregation is the strong π–π stacking between the benzene rings of the Fmoc–Cys structure.

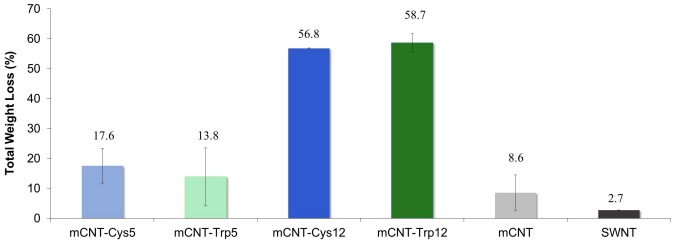

Figure 6. Total weight losses from functionalized mCNTs. a) Thermal degradation percentages from left to right for; (i) Cys5 coated mCNTs, (ii) Trp5 coated mCNTs, (iii) Cys12 coated mCNTs, (iv) Trp12 coated mCNTs, (v) uncoated mCNTs, and (vi) pristine SWCNTs.

In another previous paper published by our group, the yield of the non-covalent coating of SWCNTs with pyrene-PEG structures was investigated. This data showed the maximum functionalization percentage to be 25 %.[35] In the present study, with a switch to Fmoc-Trp and Fmoc–Cys bearing PEG conjugates, the coating yield is improved. Pyrene structure having a wider diameter may be the predominant cause of its low coating compared to Fmoc–Cys and Fmoc-Trp amino acids. With this larger diameter and thus larger volume, some C atoms can disguise from attachment. Moreover, consistent with this former publication, higher PEG molecular weights performed higher coating and hence higher thermal degradation percentages.

Magnetic Assessment of Functionalized mCNTs

The magnetic response of mCNTs to an externally applied magnetic field is significant for a targetable drug delivery system. To observe this response, Quantum Design PPMS-Vibrating Sample Magnetometry (VSM) was utilized. As shown in Figure 7, the magnetism of mCNTs before and after functionalizing with Cys5 and Cys12 was assessed. For uncoated mCNTs, we have observed a saturation magnetization (M_s) around 20 emu/g. This value indicates superparamagnetic behavior and is consistent with other mCNTs decorated with ION in the literature.[60,61] For functionalized samples of mCNTs, M_s values show a decline as expected. Specifically, Cys5-coated mCNTs show a decrease of 4 units with a 16 emu/g of saturation magnetization. Cys12 coated mCNTs on the other hand demonstrated a more intense decrease with a M_s value of 5 emu/g. The PEG causes this in Cys12 conjugates having longer chains. According to these results, all mCNT samples - uncoated or coated - are superparamagnetic and can be

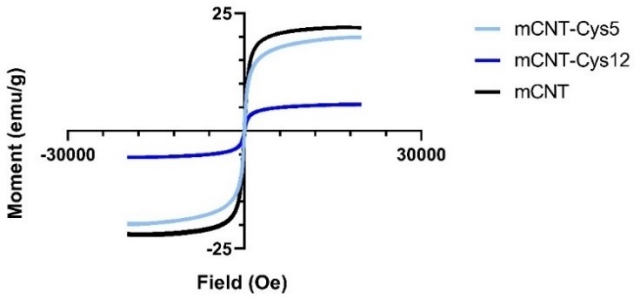

Figure 7. Hysteresis loops Cys5 coated, Cys12 coated, and pristine mCNTs.

mobilized towards the magnet with an external magnetic field and avoid agglomeration when the field is turned off.[62,63]

Dispersion of Functionalized mCNTs in Water

The purpose of the functionalization of mCNTs with PEG-Fmoc-*X* complexes is to increase the blood circulation time of the drug delivery agents as well as reduce toxicity. Since the pH of deionized water (7.37) is nearly equal to blood pH (7.35–7.45),[64] dispersion in deionized water gives us insight into the blood stay of the material (Figure 8). No precipitation was observed for the first 3 hours, and then the precipitation periods varied greatly among themselves between 3 hours and 1 week. The first sample to show signs of precipitation was mCNT-Cys5 at t = 3 hours, and the precipitation continued for 3 days. Secondly, mCNT-Trp12 started showing phase separation at 7 hours and continued precipitation for 3 days. It was recorded that after 24 hours, mCNT-Cys5, and mCNT-Trp12 were visibly separated while uncoated mCNTs, mCNT-Trp5, and mCNT-Cys12 were still stable. Uncoated mCNTs have held their solubility for 48 hours which was more than expected. mCNT-Trp5 started showing precipitation signs between 48 and 72 hours. Finally, the most stable sample mCNT-Cys12 was soluble for more than 72 hours and had a precipitation period of 1 week. The underlying reason is that the Cys structure contains bulky aromatic groups in both its Fmoc and amino acid sections; therefore, the π–π interactions with the nanotube surface were stronger. Indeed, this behavior corresponds with our former study with non-magnetized carbon nanotubes.[37] In this work, we have shown via MD simulations that the adsorption profile of Fmoc–Cys is greater than Fmoc-Trp during the 144 hours observed. As for PEG, it is highly hydrophilic, spreading its polymer chains in water. This spreading causes functionalized mCNTs to float in the aqueous medium. Therefore, the mCNT-Cys12 sample's PEG fraction having a long polymeric chain compared to mCNT-Cys5 has played an important role. However, in the case of samples containing tryptophan, mCNT-Trp5 showed a more stable performance than mCNT-Trp12. This is presumed to be caused by the dynamic behavior of Trp, being adsorbed and desorbed consecutively.[37] The interaction energy of Trp-bearing PEG molecules may not have been strong enough for the longer polymer chain to be stable. Therefore, this phenomenon should be appropriately investigated in further studies.

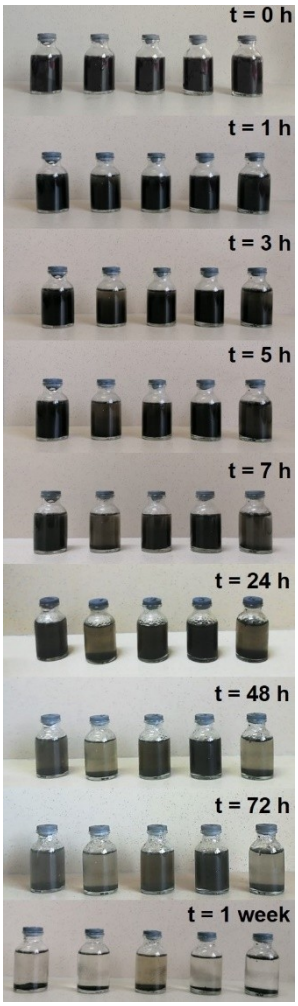

Figure 8. Precipitation behavior photographs. From left to right: (i) uncoated mCNT (control), (ii) mCNT-Cys5, (iii) mCNT-Trp5, (iv) mCNT-Cys12, (v) mCNT-Trp12.

Zeta Potential Measurements

Zeta potentials hold significance as the surface charge highly affects the nature of the sample. A less intense negative charge will potentially enhance the rate of transport of mCNTs through the cell membrane. This hypothesis is a result of the negative charge of the phospholipid layers in the cell membrane.[65] Moreover, the literature also reported that a higher zeta potential increases cell attachment patterns and results in a higher therapeutic effect.[66,67] Figure 9 shows the zeta potential of the coated and uncoated mCNTs. The negative charge of the uncoated mCNT showed a milder behavior after functionalization. This is due to PEG in the functional group having a less anionic or even neutral nature. The success of functionalization with PEG has also been shown with given zeta potentials. Also, the trend of zeta potential results is consistent with TGA results

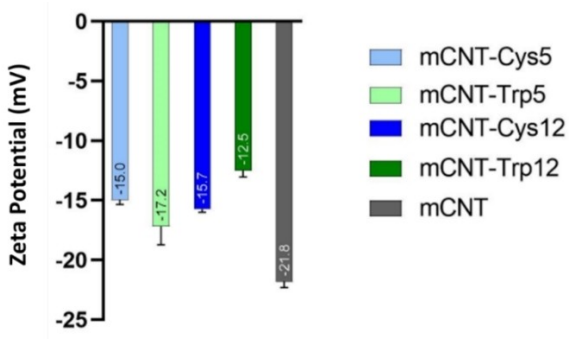

Figure 9. Overall surface charges of nanoparticles.

(Figure 6), indicating mCNT-Trp12 has the best coating yield and mCNT-Trp5 has the least successful.

Effects on Cell Viability

Among samples, Fmoc–Cys conjugated with PEG provided an increase in the solubility of mCNTs in the aquatic environment. For this reason, the effects of mCNTCys5, and mCNTCys12 on cell viability were evaluated using WST-1 assay. Figure 10 shows the survival rate of cells after treatment of human dermal fibroblast cells with 50 or 100 μg/mL of mCNT, mCNTCys5, or mCNTCys12 for 24 hours. All mCNT types significantly suppressed the cell viability of the fibroblast cells in a dose-dependent manner ($p < 0.01$). However, the toxicity of the mCNTs on the cells was slightly increased when they were coated with Cys5 or Cys12 at the lower dose. In terms of preventive effects, no significant differences were seen between Cys5 and Cys12 coated groups ($p > 0.05$).

Conclusions

A strategy of utilizing the many promising properties of CNTs while benefiting from magnetic delivery was aimed in this study. With this purpose in mind, SWCNTs are first synthesized by the CVD method. Afterward, SWCNTs were dissolved in dihydroxy benzoic acid to provide colloidal stability, and ligand exchange was applied, obtaining mCNTs magnetized with IONs.

To obtain better stability in a water medium, reduce toxicity, and obtain a more bioavailable form of mCNTs, we implemented an approach of non-covalent functionalization with two different PEG-Fmoc-amino acid complexes. An absence of Fmoc–Cys attachment to graphitic surfaces was noticed in the literature. Therefore, our group had a rather comparative point of view between Fmoc-Trp and Fmoc–Cys structures regarding their success and yield of functionalizing lateral surfaces of mCNTs. The effect of PEG chain length was included in the study to observe the effect of a bioavailable and hydrophilic polymer. Samples that contained Fmoc–Cys have given a low yield of mCNT surface functionalization in comparison with Fmoc-Trp. Nonetheless, this lesser yield is hypothesized to result from the extra aromatic rings in the Fmoc–Cys structure, taking up volume and hiding neighbor C atoms. Fmoc–Cys which were conjugated with PEG showed an increase in the solubility of mCNTs with dispersion experiments. Thus, the answer to the research question was given; it has been shown that non-covalent attachment of Fmoc-PEGs to iron oxide-decorated single-walled CNTs is possible. In brief, the overall results of this study have given many hints that functionalized mCNTs may be used in therapeutic applications such as cancer research and therapy, enabling magnetic delivery and high availability.

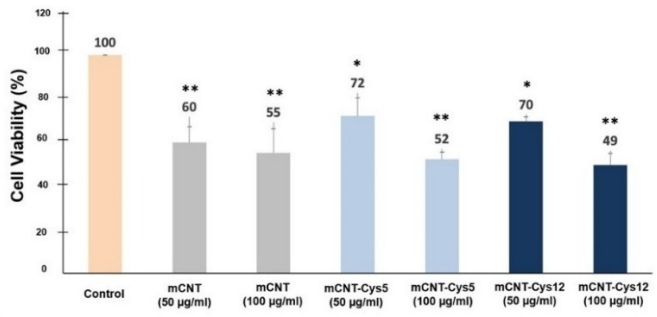

Figure 10. The effects of mCNTs on cell viability. The cells were treated with various concentrations (50, 100 μL/mL) of mCNTs coated or not coated with Cys5 or Cys12 for 24 hours. The percentage of cell viability was measured with the WST-1 assay. Data are the mean values for triplicate experiments. *$p < 0.01$, **$p < 0.001$ compared to the control.

Experimental Section

Materials

PEG_{5000} and PEG_{12000} were obtained from Sigma-Aldrich and used as received. Fmoc–Cys (95%) and Fmoc-Trp (97%), 4-(dimethylamino) pyridine (DMAP), and N, N′-dicyclohexylcarbodiimide (DCC) were all procured from Sigma Aldrich as well and used as arrived. Solvents such as THF (99.8%), dichloromethane (DCM; 99.8%), and diethyl ether (Et_2O; 99.7%) were bought from Sigma-Aldrich and used without any purification procedures.

Methods

The following headlines aim to outline the methods employed in this study. To maintain clarity and simplicity, we have encapsulated the steps involved in the preparation steps in Figure 11.

Synthesis and Purification of Single-Walled Carbon Nanotubes

SWCNTs were synthesized by using the CVD process as described previously by Karatepe et al..[68] After the synthesis, SWCNTs were treated with 6 M HNO_3 at 120 °C for 3 h to remove metal catalyst particles. Then the purified sample was washed with distilled water until pH reached a neutral level and then dried in an oven at 105 °C for 48 hours.

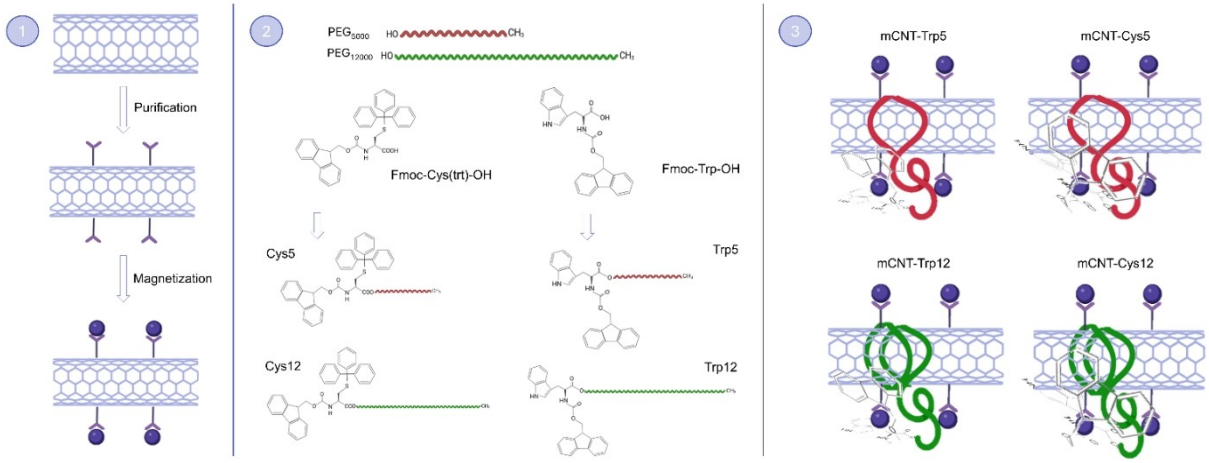

Figure 11. To prepare Fmoc amino acid-modified PEG-coated magnetic SWCNTs, follow these steps: 1. Purification of the SWCNTs after synthesis to provide functional groups on their surface. 2. Esterification reaction with Fmoc-protected amino acid and PEG to obtain Fmoc Amino Acid-Modified Polyethylene Glycol. There are two types of Fmoc-protected amino acids - cysteine and tryptophan - and two lengths of PEG - 5000 and 12000. 3. Coating the Fmoc Amino Acid-Modified Polyethylene Glycol onto magnetic SWCNTs to obtain coated mCNTs.

Synthesis of Iron Oxide Nanoparticles

The synthesis of IONs was carried out similarly to a previous report.[69] $FeCl_3$ and $FeSO_4.7H_2O$ were dissolved in deionized water. At 25 °C, ammonium hydroxide was slowly added to the solution. The solution was magnetically stirred for a certain amount of time allowing the precipitation of the nanoparticles. The precipitate was separated with the help of a magnet, decanted, and washed with deionized water until the pH reached neutral. Then it was dried using a freeze-dryer for 24 hours.

IONs were then coated with oleic acid, a type of fatty acid, to endow nanoparticles' colloidal stability in organic solvents. The nanoparticles were first added to the 3 M ammonium hydroxide solution. After mixing for a while with the help of a mechanical stirrer, oleic acid was added to the solution, and the mixing continued for another 15 minutes at 1000 rpm. Coated magnetic nanoparticles were separated by a magnet. It was washed with distilled water and ethanol to remove ammonium hydroxide and excess oleic acid. Then the sample was freeze-dried overnight.

Modification of SWCNTs with IONs

Magnetically modified SWCNTs were prepared by the ligand exchange method.[70] SWCNTs were dispersed for 30 minutes in 20 mL THF with the help of an ultrasonic probe. A second solution was prepared in 15 mL THF with magnetic nanoparticles coated with oleic acid. These solutions were mixed so that the nanotube/iron oxide ratio was 2:1 and stirred at 700 rpm for 6 hours. Then the mCNTs were collected with a magnet and freeze-dried overnight.

Preparation of PEG-Fmoc Amino Acid Complexes

Conjugation of PEG and Fmoc-amino acids molecules has been done by direct esterification, as explained in the literature.[37,71] To briefly narrate, PEG_{5000} (2 g, 0.4 mmol) is completely dissolved in 30 mL of DCM. Fmoc–Cys (0.32 g, 0.546 mmol), DMAP (0.024 g, 0.196 mmol), and DCC (0.15 g, 0.727 mmol) are added. Thus, Fmoc–Cys and PEG_{5000} conjugates (Cys5) were obtained. For the second sample, the same procedure was applied using 0.26 g (0.610 mmol) of Fmoc-Trp instead of Fmoc–Cys. Hence Trp5 is obtained. Then, 20 mL of DCM is added to the mixtures. The solutions were left to mix for 72 hours. A portion of the mixed solutions was concentrated in a rotary evaporator and then precipitated in diethyl ether. The precipitates were dissolved again in DCM and precipitated in diethyl ether two times, aiming for extra purification. Lastly, the resulting whitish solutes were left to dry at room temperature for 24 hours. The same method was used to synthesize the samples of Cys12 and Trp12 considering molar equivalents.

Functionalization of mCNTs with PEG-Fmoc Amino Acids

PEG-Fmoc amino acid complexes (0.25 g) were dissolved in 50 mL of THF. In each solution, mCNTs (0.05 g, 5 w/w polymers to nanotubes ratio) were added. Each sample was ultrasonicated for 30 minutes and then stirred in mechanical stirrers for 7 days. After the solutions obtained were filtered with polymer filter paper (Sartorius, pore size: 0.2 um), they were refiltered with 25 mL of THF for extra separation. Lastly, the remaining precipitates were left to dry at 32 °C for 24 hours. With this technique, functionalized mCNTs as black, dust-like particles were obtained. Coding of the coated samples is done in the form mCNT*aaX* (Table 1). Here *aa* represents the type of Fmoc-amino acid, and *X* represents 1/1000th of the molecular weight of PEG.

Table 1. Code of Samples.

Code	Fmoc-amino acid	PEG
mCNT-Trp5	Fmoc-Trp-OH	PEG5000
mCNT-Trp12	Fmoc-Trp-OH	PEG12000
mCNT-Cys5	Fmoc–Cys(trt)-OH	PEG5000
mCNT-Cys12	Fmoc–Cys(trt)-OH	PEG12000

Characterization of Materials

All PEG-Fmoc-amino acid complexes were characterized by FTIR spectroscopy and ^{1}H NMR analysis. For FTIR spectra, a Perkin-Elmer (Waltham, MA) Spectrum One with an ATR system is used. ^{1}H NMR spectra were collected with an Agilent V NMRS 500 device (500 MHz for 1H) and the samples were gathered in $CDCl_3$ with $Si(CH_4)$. To characterize functionalized mCNTs, fluorescence spectra are acquired with Hitachi F-4500 spectrophotometry using DCM as the solvent. FEG-SEM was done with FEI Quanta 450 FEG device in ESEM mode. TGA is executed with a Perkin-Elmer Diamond TA/TGA device between the temperature range of 30–800 °C in an inert atmosphere (N_2) with a heating velocity of 10 °C/min. DXR Raman model of Thermo Scientific with 532 nm laser was used in the study. Raman analysis is carried out at room temperature without pre-preparation. XRD analyses of the synthesized samples were performed with the PAN analytical - X'Pert Pro device. XRD data were obtained using 1.5406 nm Cu Kα radiation. The 2θ range used for analysis is between 10–80°. The magnetic behavior of mCNTs before and after functionalization is assessed using a VSM device to a maximum field of 30 kOe (3 T). VSM was utilized at room temperature while cycling the field between −30000 and 30000 Oe. For dispersion tests, 4 types of coated mCNTs and uncoated mCNTs (control), a total of 5 samples (5 mg each) are dispersed in 5 mL water via 30 minutes ultra-sonication. Afterward, the samples are placed in homogenous conditions, and their precipitation behaviors are photographed. The photographs were taken at t = 0, t = 1 hour, t = 3 hours, t = 5 hours, t = 7 hours, t = 24 hours, t = 48 hours, t = 72 hours, and t = 1 week. Zeta potential measurements were performed in a folded capillary cell using a Zetasizer (Zetasizer Nano ZS, Malvern, UK) instrument equipped with 4.0 mV He–Ne laser lamp (633 nm) at 25 °C with ±0.1 °C sensitivity with DLS and electrophoretic light scattering (ELS) techniques, respectively. Measurements were taken after each sample (1 mg/mL) was dispersed in deionized water using an ultrasonic probe for 30 minutes.

Cell Viability

To evaluate the effects of the mCNTs on cell viability, a WST-1 assay was performed (Roche, Mannheim, Germany) according to the manufacturer's instructions. PCS-201–012 human dermal fibroblast cells (ATCC) were cultured in RPMI 1640 medium, supplemented with FBS (10 %), penicillin (100 units/mL), and streptomycin (100 μg/mL) at 37 °C in a humidified atmosphere of 5 % CO_2. For the assay, first, the cells were seeded into a 96-well plate and allowed to attach to the plate overnight. After the cells were treated with uncoated mCNTs, mCNT-Cys5 or mCNT-Cys12 with different concentrations (50, 100 μL/mL) for 24 hours, the samples were removed, and a fresh medium was added to per well. 5 μL/well WST-1 cell proliferation reagent was added to each well, and the plate was incubated in a CO_2 incubator at 37 °C for 3 hours. The absorbances of the wells were measured at 440 nM with a microplate reader (Molecular Devices, CA, USA). The control group consisted of cells that were not treated with mCNTs, mCNT-Cys5, or mCNT-Cys12. The viability of the cells was expressed as a percentage relative to the value of control cells. Statistical analysis was performed using IBM SPSS Statistics 13.0 (Chicago, IL, USA). The data were subjected to one-way ANOVA to evaluate the differences between the groups.

Supporting Information

The authors have given additional figures within the Supporting Information.

Acknowledgements

This work was funded by Istanbul Technical University Scientific Research Projects Foundation, Project No. MGA-2019–41823.

Conflict of Interests

The authors declare no conflict of interest.

Keywords: Single-walled carbon nanotube · Iron oxide · Fmoc amino acid · Polyethylene glycol · Surface functionalization

[1] B. Abdallah, A. M. A. Elhissi, W. Ahmed, M. Najlah in *Advances in Medical and Surgical Engineering*, (Eds. W. Ahmed, D. A. Phoenix, M. J. Jackson, C. P. Charalambous), Academic Press, **2020**, pp. 313–332.
[2] S. M. Aberoumandi, M. Mohammadhosseini, E. Abasi, S. Saghati, N. Nikzamir, A. Akbarzadeh, Y. Panahi, S. Davaran, *Nanomedicine Biotechnol.* **2017**, *45*, 1058–1068.
[3] Y.-J. Lu, K.-C. Wei, C.-C. M. Ma, S.-Y. Yang, J.-P. Chen, *Colloids Surf. B. Biointerfaces.* **2012**, *89*, 1–9.
[4] P. Ghoderao, S. Sahare, P. Alegaonkar, A. A. Kulkarni, T. Bhave, *ACS Appl. Nano Mater.* **2019**, *2*, 607–616.
[5] H. Xu, L. Wang, J. Luo, Y. Song, J. Liu, S. Zhang, X. Cai, *Sensors.* **2015**, *15*, 1008–1021.
[6] K. Elumeeva, M. A. Kazakova, D. M. Morales, D. Medina, A. Selyutin, G. Golubtsov, Y. Ivanov, V. Kuznetzov, A. Chuvilin, H. Antoni, M. Muhler, W. Schuhmann, J. Masa, *ChemSusChem.* **2018**, *11*, 1204–1214.
[7] U. Carragher, D. Branagan, C. B. Breslin, *Materials.* **2019**, *12*, 2587.
[8] A. Masotti, A. Caporali, *Int. J. Mol. Sci.* **2013**, *14*, 24619–24642.
[9] C. Guilbaud-Chéreau, B. Dinesh, R. Schurhammer, D. Collin, A. Bianco, C. Ménard-Moyon, *ACS Appl. Mater. Interfaces.* **2019**, *11*, 13147–13157.
[10] A. Servant, I. Jacobs, C. Bussy, C. Fabbro, T. da Ros, E. Pach, B. Ballesteros, M. Prato, K. Nicolay, K. Kostarelos, *Carbon N. Y.* **2016**, *97*, 126–133.
[11] B. Chen, H. Zhang, N. Du, B. Zhang, Y. Wu, D. Shi, D. Yang, *J. Colloid Interface Sci.* **2012**, *367*, 61–66.
[12] M.-L. Chen, Y.-J. He, X.-W. Chen, J.-H. Wang, *Langmuir.* **2012**, *28*, 16469–16476.
[13] D. Xiao, P. Dramou, H. He, L. A. Pham-Huy, H. Li, Y. Yao, C. Pham-Huy, *J. Nanoparticle Res.* **2012**, *14*, 984.
[14] D. Yang, F. Yang, J. Hu, J. Long, C. Wang, D. Fu, Q. Ni, *Chem. Commun.* **2009**, 4447–4449.
[15] X. An, H. Wu, Y. Li, X. He, L. Chen, Y. Zhang, *Talanta.* **2020**, *210*, 120632.
[16] P. M. Price, W. E. Mahmoud, A. A. Al-Ghamdi, L. M. Bronstein, *Front. Chem.* **2018**, *6*,1–7.
[17] S. Boncel, A. P. Herman, S. Budniok, R. G. Jędrysiak, A. Jakóbik-Kolon, J. N. Skepper, K. H. Müller, *ACS Biomater. Sci. Eng.* **2016**, *2*, 1273–1285.
[18] C. S. Sharma, S. Sarkar, A. Periyakaruppan, J. Barr, K. Wise, R. Thomas, B. L. Wilson, G. T. Ramesh, *J. Nanosci. Nanotechnol.* **2007**, *7*, 2466–2472.
[19] E. Herzog, A. Casey, F. M. Lyng, G. Chambers, H. J. Byrne, M. Davoren, *Toxicol. Lett.* **2007**, *174*, 49–60.
[20] L. Ding, J. Stilwell, T. Zhang, O. Elboudwarej, H. Jiang, J. P. Selegue, P. A. Cooke, J. W. Gray, F. F. Chen, *Nano Lett.* **2005**, *5*, 2448–2464.
[21] T. Pellegrino, L. Manna, S. Kudera, T. Liedl, D. Koktysh, A. L. Rogach, S. Keller, J. Rädler, G. Natile, W. J. Parak, *Nano Lett.* **2004**, *4*, 703–707.
[22] E. E. Lees, T.-L. Nguyen, A. H. A. Clayton, B. W. Muir, P. Mulvaney, *ACS Nano.* **2009**, *3*, 1121–1128.
[23] M. Panagiotopoulou, Y. Salinas, S. Beyazit, S. Kunath, L. Duma, E. Prost, A. G. Mayes, M. Resmini, B. Tse Sum Bui, K. Haupt, *Angew. Chemie Int. Ed.* **2016**, *55*, 8244–8248.

[24] Z. Spitalsky, D. Tasis, K. Papagelis, C. Galiotis, *Prog. Polym. Sci.* **2010**, *35*, 357–401.
[25] A. Antonucci, J. Kupis-Rozmysłowicz, A. A. Boghossian, *ACS Appl. Mater. Interfaces.* **2017**, *9*, 11321–11331.
[26] L. Y. Yan, Y. F. Poon, M. B. Chan-Park, Y. Chen, Q. Zhang, *J. Phys. Chem. C.* **2008**, *112*, 7579–7587.
[27] A. Ishibashi, N. Nakashima, *Chemistry.* **2006**, *12*, 7595–7602.
[28] H. Dodziuk, A. Ejchart, W. Anczewski, H. Ueda, E. Krinichnaya, G. Dolgonos, W. Kutner, *Chem. Commun.* **2003**, 986–987.
[29] K. V. Singh, R. R. Pandey, X. Wang, R. Lake, C. S. Ozkan, K. Wang, M. Ozkan, *Carbon N. Y.* **2006**, *44*, 1730–1739.
[30] S. Daniel, T. P. Rao, K. S. Rao, S. U. Rani, G. R. K. Naidu, H. Y. Lee, T. Kawai, *B Chem.* **2007**, *122*, 672–682.
[31] A. K. Varkouhi, S. Foillard, T. Lammers, R. M. Schiffelers, E. Doris, W. E. Hennink, G. Storm, *Int. J. Pharm.* **2011**, *416*, 419–425.
[32] A. A. Bhirde, S. Patel, A. A. Sousa, V. Patel, A. A. Molinolo, Y. Ji, R. D. Leapman, J. S. Gutkind, J. F. Rusling, *Nanomedicine.* **2010**, *5*, 1535–1546.
[33] A. Star, J. F. Stoddart, D. Steuerman, M. Diehl, A. Boukai, E. W. Wong, X. Yang, S.-W. Chung, H. Choi, J. R. Heath, *Angew. Chem. Int. Ed. Engl.* **2001**, *40*, 1721–1725.
[34] F. Cheng, A. Adronov, *Chem. – A Eur. J.* **2006**, *12*, 5053–5059.
[35] M. Meran, P. D. Akkus, O. Kurkcuoglu, E. Baysak, G. Hizal, E. Haciosmanoglu, A. Unlu, N. Karatepe, F. S. Güner, *Langmuir.* **2018**, *34*, 12071–12082.
[36] S. Roy, A. Banerjee, *RSC Adv.* **2012**, *2*, 2105–2111.
[37] Y. Yeniyurt, S. Kilic, Ö. Z. Güner-Yılmaz, S. Bozoglu, M. Meran, E. Baysak, O. Kurkcuoglu, G. Hizal, N. Karatepe, S. Batirel, F. S. Güner, *Front. Bioeng. Biotechnol.* **2021**, *9*, 648366.
[38] L. Shen, H. Song, H. Cui, X. Wen, X. Wei, C. Wang, *CrystEngComm.* **2013**, *15*, 9849–9854.
[39] Y. Liu, N. Wu, Z. Wang, H. Cao, J. Liu, *New J. Chem.* **2017**, *41*, 6241–6250.
[40] A. Medina, F. A. Casado-Carmona, Á. I. López-Lorente, S. Cárdenas, *Nanomaterials.* **2020**, *10*.
[41] X.-Q. Li, P.-X. Hou, C. Liu, H.-M. Cheng, *Carbon N. Y.* **2019**, *147*, 187–198.
[42] B. A. Chambers, C. J. Shearer, L. Yu, C. T. Gibson, G. G. Andersson, *Nanomaterials.* **2018**, *8*.
[43] H. Yau, M. K. Bayazit, J. Steinke, M. Shaffer, *Macromolecules.* **2014**, *47*, 4870–4875.
[44] J. Seo, W. Hoffmann, S. Warnke, X. Huang, S. Gewinner, W. Schöllkopf, M. T. Bowers, G. von Helden, K. Pagel, *Nat. Chem.* **2017**, *9*, 39–44.
[45] K. Abe, K. Higashi, K. Watabe, A. Kobayashi, W. Limwikrant, K. Yamamoto, K. Moribe, *Col.l Surf. A Physicochem. Eng. Asp.* **2015**, *474*.
[46] N.-H. Yao, W.-Y. He, K. S. Lam, G. Liu, *J. Comb. Chem.* **2004**, *6*, 214–219.
[47] M. Uygun, M. A. Tasdelen, Y. Yagci, *Macromol. Chem. Phys.* **2010**, *211*, 103–110.
[48] D. Wang, W. X. Ji, Z. C. Li, L. Chen, *J. Am. Chem. Soc.* **2006**, *128*, 6556–6557.
[49] Y. Gao, M. Shi, R. Zhou, C. Xue, M. Wang, H. Chen, *Nanotechnology.* **2009**, *20*.
[50] Y. Li, B. G. Cousins, R. V. Ulijn, I. A. Kinloch, *Langmuir.* **2009**, *25*, 11760–11767.
[51] S. M. M. Reddy, G. Shanmugam, N. Duraipandy, M. S. Kiran, A. B. Mandal, *Soft Matter.* **2015**, *11*, 8126–8140.
[52] K. M. Liew, C. H. Wong, X. Q. He, M. J. Tan, *Phys. Rev. B.* **2005**, *71*, 75424.
[53] I. M. Weiss, C. Muth, R. Drumm, H. O. K. Kirchner, *BMC Biophys.* **2018**, *11*, 2.
[54] F. Basile, S. Zhang, S. K. Kandar, L. Lu, *J. Am. Soc. Mass Spectrom.* **2011**, *22*, 1926–1940.
[55] N. Vrandečić, M. Erceg, M. Jakić, I. Klarić, *Thermochim. Acta.* **2010**, *498*, 71–80.
[56] W.-D. Li, E.-Y. Ding, *Sol. Energy Mater. Sol. Cells.* **2007**, *91*, 764–768.
[57] D. Andrade, C. Moya, F. Olate, N. Gatica, S. Sanchez, E. Díaz, E. Elgueta, M. Parra, M. Dahrouch, *RSC Adv.* **2016**, *6*, 38505–38514.
[58] A. C. V. Araújo, R. de Oliveira, S. Alves, A. Rodrigues, F. Machado, F. A. O. Cabral, W. De Azevedo, *Synth. Met.* **2010**, *160*, 685–690.
[59] A. Gemeay, B. E. Keshta, R. El-Sharkawy, A. Zaki, *Environ. Sci. Pollut. Res.* **2020**, *27*.
[60] M. R. Islam, M. Ferdous, M. I. Sujan, X. Mao, H. Zeng, M. S. Azam, *J. Colloid Interface Sci.* **2020**, *562*, 52–62.
[61] E. Kılınç, *J. Magn. Magn. Mater.* **2016**, *401*, 949–955.
[62] N. N. Al-Rawi, B. A. Anwer, N. H. Al-Rawi, A. T. Uthman, I. S. Ahmed, *Saudi Pharm. J. SPJ Off. Publ. Saudi Pharm. Soc.* **2020**, *28*, 876–887.
[63] D. W. Chakeres, F. de Vocht, *Prog. Biophys. Mol. Biol.* **2005**, *87*, 255–265.
[64] J. A. Kellum, *Crit. Care.* **2000**, *4*, 6–14.
[65] M. Pekker, M. N. Shneider, *ArXiv Prepr.* **2014**, 5.
[66] U. Bozuyuk, N. O. Dogan, S. Kizilel, *ACS Appl. Mater. Interfaces.* **2018**, *10*, 33945–33955.
[67] A. Doostmohammadi, A. Monshi, R. Salehi, M. H. Fathi, Z. Golniya, A. U. Daniels, *Ceram. Int.* **2011**, *37*, 2311–2316.
[68] E. Dündar-Tekkaya, N. Karatepe, *Fuller. Nanotub. Car. N.* **2015**, *23*, 535–541.
[69] C. wei Lai, L. Foo, F. W. Low, M. Foong, S. Bee, A. Hamid, *Adv. Polym. Technol.* **2017**, *1*.
[70] G. Lamanna, A. Garofalo, G. Popa, C. Wilhelm, S. Bégin-Colin, D. Felder-Flesch, A. Bianco, F. Gazeau, C. Ménard-Moyon, *Nanoscale.* **2013**, *5*, 4412–4421.
[71] D. Niculescu-Duvaz, J. Getaz, C. J. Springer, *Bioconjug. Chem.* **2008**, *19*, 973–981.

Manuscript received: January 14, 2024
Revised manuscript received: April 23, 2024
Accepted manuscript online: April 26, 2024
Version of record online: ■■, ■■

RESEARCH ARTICLE

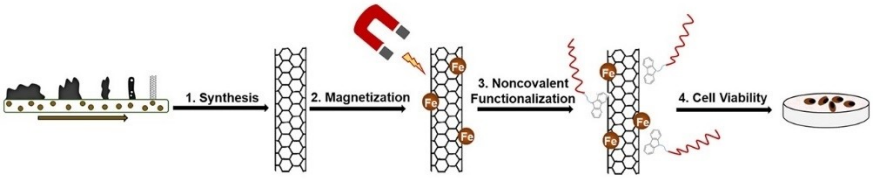

*F. Sevval Murat, Ö. Z. Güner-Yılmaz, S. Bozoglu, Assoc. Prof. S. Batirel, E. Baysak, Prof. Dr. G. Hizal, Prof. Dr. N. Karatepe, Prof. Dr. F. Seniha Güner**

1 – 10

Non-Covalent Functionalization of Magnetic Carbon Nanotubes with Fmoc Amino Acid-Modified Polyethylene Glycol

In order to address dispersion issues and enhance stability of carbon nanotubes decorated with iron oxide (mCNTs) in a water environment, a strategy involving non-covalent functionalization with two distinct complexes of poly(ethylene glycol)-Fmoc-amino acids is employed. The findings of this investigation strongly suggest that functionalized mCNTs hold promise for therapeutic endeavors like cancer research and treatment, facilitating magnetic delivery and improving accessibility.